First-principles study of the elasticity, piezoelectricity, and vibrational modes in $LiGaO_2$ compared with ZnO and GaN

Adisak Boonchun and Walter R. L. Lambrecht
Department of Physics, Case Western Reserve University, Cleveland, Ohio 44106-7079, USA
(Received 25 February 2010; revised manuscript received 14 May 2010; published 23 June 2010)

The lattice-dynamical properties of $LiGaO_2$ have been studied by means of first-principles density-functional calculations using the pseudopotential linear-response approach in the local-density approximation. For comparison, similar calculations are performed for the related materials ZnO and GaN. The quantities calculated are the elastic constants, the piezoelectric constants, the static and high-frequency dielectric constants, and the zone-center vibrational modes. The latter are used to calculate infrared optical spectra and compared with experiment. The results are compared to available experimental data, indicating overall satisfactory agreement typical of the methodology used. The nature of the vibrational modes is examined in terms of the mode eigenvectors and indicates a large mixing of wurtzite derived modes due to the lower symmetry.

DOI: 10.1103/PhysRevB.81.235214 PACS number(s): 78.30.Hv, 63.20.dk, 62.20.de, 77.65.Bn

I. INTRODUCTION

Recently, there has been a renewed interest in tetrahedrally bonded oxides, such as ZnO and related alloys (e.g., $Zn_xMg_{1-x}O$) for various optoelectronic properties, transparent conducting oxides, etc. Closely related to ZnO is the material $LiGaO_2$, which can be thought of as related to ZnO by replacing the group II element Zn by a group III (Ga) and a group I element Li in an ordered arrangement. $LiGaO_2$ has been explored as a suitable substrate for GaN (Refs. 1–4) and ZnO thin-film growth.[5] Not only is the basal plane lattice mismatch less than 1% but also large crystals can be grown by the Czochralsky method.[6] Furthermore, heteroepitaxial growth of $LiGaO_2$ on ZnO has been achieved.[7] Surface properties of $LiGaO_2$ and etching have been investigated in relation to their use in epitaxial growth.[8–10] Even mixed alloys of $LiGaO_2$ and ZnO have been reported.[11] $LiGaO_2$ was considered in the past for nonlinear optical properties[12–14] and is also a promising material for ultrasonic devices, such as resonators and transducers because it has a piezoelectric effect with high coupling coefficient.[15,16] Limpijumnong *et al.*[17] did the first band-structure calculations using first-principles calculations and considered different wurtzite-derived crystal structures for $LiGaO_2$. They showed that the important factor for the bonding is the exclusive occurrence of Li_2Ga_2 tetrahedra surrounding oxygen. Although experimental data for the elastic constant, piezoelectric constants, and various optical properties, related to the vibrational modes (Raman and infrared reflectivity) have been available in literature for some time,[14,15] no attempts have been made to obtain these properties from first-principles calculations.

The purpose of this paper is to present a comprehensive computational study of the lattice-dynamical properties of this material in comparison with those of ZnO and GaN. First, a comparison of calculated properties for perfect material with experimental results may give insight in the quality of the crystals that were used in those experiments and in the accuracy of the measurements. In particular, only a few groups have reported results on these materials, so their properties are not yet well established. Second, a comprehensive study may provide insights in the relations between these properties and gives us access to quantities difficult to measure, such as the individual phonon modes. We use the linear-response approach in the local-density approximation (LDA) to calculate elastic, piezoelectric and dielectric properties, and vibrational modes of orthorhombic $LiGaO_2$ and compare them with the available experimental data. Another reason for our interest in these materials is that their crystal structure is isomorphic to that of the Zn-IV-N_2 semiconductors for which we recently presented comprehensive studies of the vibrational and related properties.[18–21] Unlike those materials, which are only available in thin film or needle form, $LiGaO_2$ is available as large single crystals and thus a more complete set of data on vibrational modes for different symmetries is available. It is also of interest to study the relationship of the properties in this material with those in the parent compound ZnO and because of the close lattice mismatch to GaN, we also perform some related calculations on GaN for comparison.

II. COMPUTATIONAL METHOD

The underlying computational approach of this paper is density-functional theory.[22,23] The computational method used to apply this theory is the plane-wave pseudopotential iterative minimization approach[24] as implemented in the ABINIT package.[25]

However, besides the total energies and structural relaxation, we are here also interested in calculating various derivatives of the total energy. For instance, to calculate vibrational modes, we need force constants, which are second derivatives of the total energy versus atomic displacements, to calculate elastic constants, we need derivatives versus uniform strain and to calculate piezoelectric constants, and we need polarization, which is a derivative of the total energy versus electric field. To obtain these various derivatives, the ABINIT package uses the density-functional perturbation theory (DFPT).[26–28] The approach of Hamann *et al.*[29] is used to deal systematically with strains and piezoelectric effects are treated as defined in Wu *et al.*[30]

The LDA in the Perdew-Zunger[31] parametrization was used for the exchange and correlation energy. While the gen-

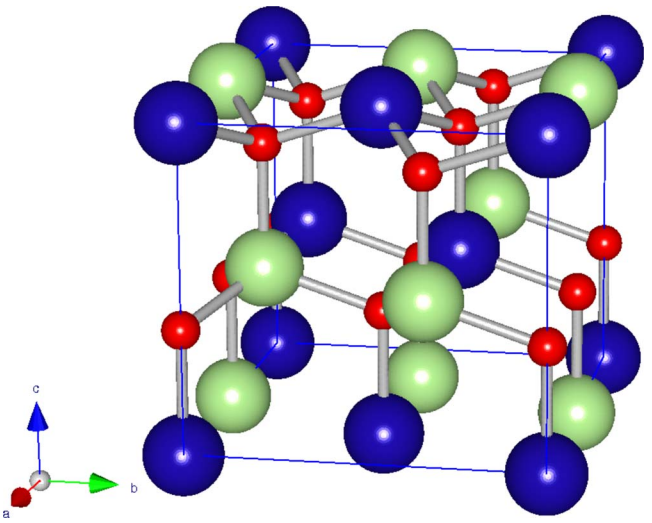

FIG. 1. (Color online) Crystal structure of $LiGaO_2$, small red spheres O, large dark blue spheres Li, and large light green spheres Ga.

eralized gradient approximation (GGA) has recently become more popular, it is not clear which of the two gives the better results for elastic constants or vibrational modes. GGA tends to overestimate lattice constants slightly while LDA underestimates them, so LDA overestimates and GGA underestimates the bonding strength. As we will show, the LDA provides fairly accurate lattice constants for these materials and is thus suitable for this study. Neither GGA nor LDA provides good band gaps. Therefore the study of the electronic band structure is not emphasized here and left for a future study using the more accurate GW (Green's function G and screened Coulomb interaction W) approach. Here we focus on ground-state properties.

We use norm conserving Fritz-Haber pseudopotentials[32] The $3d$ electrons of Ga were treated as valence electrons. The calculations were carried out with a 60 Ry plane-wave energy cutoff and the orthorhombic Brillouin zone was sampled with a regular and shifted $6\times6\times6$ k-point mesh. Our tolerance for convergence of the squared residual of the wave functions $(\langle\psi|(H-E)^2|\psi\rangle$ with $E=\langle\psi|H|\psi\rangle)$ is 10^{-18} hartree^2 while for the forces it is 10^{-6} hartree/bohr.

III. RESULTS

A. Lattice parameters

The orthorhombic crystal structure of $LiGaO_2$ is closely related to the wurtzite structure as follows: $\mathbf{a}\approx2\mathbf{a}_1^{wz}$, $\mathbf{b}\approx\mathbf{a}_1^{wz}+2\mathbf{a}_2^{wz}$, and $\mathbf{c}=\mathbf{c}^{wz}$. Here, $\mathbf{a}_2^{wz}$ is at an angle of 120° from the $\mathbf{a}_1^{wz}$. The Li and Ga atoms are ordered in a particular way in the cation sublattice as shown in Fig. 1. The space group is $Pna2_1$ and the atoms occur in 4(a) Wyckoff positions.

When the twofold screw axes along the z direction is chosen to pass through the origin of the unit cell, the reduced coordinates of each type of atom are (x,y,z), $(\bar{x},\bar{y},\frac{1}{2}+z)$, $(\frac{1}{2}-x,\frac{1}{2}+y,z)$, and $(\frac{1}{2}+x,\frac{1}{2}-y,\frac{1}{2}+z)$, with x,y,z given in Table I. Note that we have reversed the a and b axes from the conventional definition of the space group to more clearly see the relation to wurtzite. Our choice corresponds to $a>b>c$. With our choice of axes, the space group should be labeled $Pnb2_1$.

TABLE I. Reduced coordinates of the atoms in $LiGaO_2$.

	Atom	x	y	z
Present calculation	Ga	0.1241	0.0818	0
	O_I	0.1177	0.4178	0.8850
	O_{II}	0.1323	0.0876	0.3760
	Li	0.1255	0.4160	0.4970
Experiment[a]	Ga	0.1263	0.0821	0
	O_I	0.1388	0.4066	0.8927
	O_{II}	0.1121	0.0697	0.3708
	Li	0.1267	0.4207	0.4936

[a]Reference 33.

Table II shows the calculated lattice constants, band-gap energy, average bond lengths, and bond angles, compared with the experimental results. We can see that lattice constants of the orthorhombic structure are obtained in agreement with experiment to better than 2% and the internal positions are also in excellent agreement.

Because of the close relation to GaN and ZnO, we also show our calculated lattice properties for GaN and ZnO obtained within the same approach in Table III. We find indeed a lattice match to within 2% with the lattice constant of GaN and ZnO. The $LiGaO_2$ a lattice constant divided by two corresponds to the wurtzite lattice constant and is 3.1275 Å. However, the lattice match is better between ZnO and GaN than between $LiGaO_2$ with either of the two. Also, note that the b/a ratio in $LiGaO_2$ is 0.857 rather than $\sqrt{3}/2=0.866$ the ideal ratio derived from the parent wurtzite structure. The ratio $2c/a$ is 1.5836 which is significantly smaller than the wurtzite c/a of ZnO or GaN. Thus, there is good lattice match in a direction of the basal plane but somewhat larger mismatch −3.2% for the b direction or c direction (−3.3%) with ZnO. With GaN, the mismatches in a, b, and c directions are −2%, −3%, and −4.5%.

$LiGaO_2$ is a wide-band gap and direct-gap semiconductor. Its experimental direct band-gap energy is 5.6 eV.[7] The gap

TABLE II. Calculated lattice constants (Å), bond lengths (Å), and bond angles (°) of $LiGaO_2$, compared to experimental data.

		Calc.	Expt.[a]
Lattice constant	a	6.255	6.372
	b	5.361	5.402
	c	4.953	5.007
Band gap energy		3.136	5.6[b]
Average bond lengths	Ga-O	1.858	1.848
	Li-O	1.923	1.985
Bond angles	Ga-O-Ga	112.3	109.2
	Li-O-Li	107.5	103.3

[a]Reference 33.
[b]From Ohkubo *et al.* (Ref. 7), and references therein.

TABLE III. Lattice constants of wurtzite ZnO and GaN.

	Method	a	c/a	u
ZnO	DFT[a]	3.199	1.612	0.379
	DFT[b]	3.197	1.616	0.380
	Hartree Fock	3.286	1.595	0.383
	Expt.	3.250	1.602	0.382
GaN	DFT	3.19	1.63	0.376
	DFT-LMTO[c]	3.17	1.62	0.379
	Expt.	3.189	1.625	

[a]Present work.
[b]From Wu *et al.* (Ref. 30).
[c]From Kim *et al.* (Ref. 34).

obtained from our calculations is 3.136 eV. This close to the results reported earlier, 3.415 eV by Limpijumnong *et al.*[17] with a different band-structure approach. As usual LDA underestimates the band gap. One expects the band-gap correction to be similar to that in ZnO. For ZnO, the LDA gap is 0.81 eV and the experimental gap is 3.4 eV.[35] Assuming a similar correction one would obtain a gap of 5.7 eV for $LiGaO_2$ in close agreement with the experiment. Since this paper is focused on lattice-dynamical properties, which are electronic ground-state properties, rather than electronic excited-state properties, we do not discuss the band structure in further detail. A discussion of the band structure can be found in Ref. 17.

B. Elastic constants

In accordance with the orthorhombic crystal structure and the point symmetry group C_{2v}, there are nine distinct elastic constants. The stress and stain tensors are related by

$$\begin{bmatrix} \sigma_1 \\ \sigma_2 \\ \sigma_3 \\ \sigma_4 \\ \sigma_5 \\ \sigma_6 \end{bmatrix} = \begin{bmatrix} c_{11} & c_{12} & c_{13} & 0 & 0 & 0 \\ c_{12} & c_{22} & c_{23} & 0 & 0 & 0 \\ c_{13} & c_{23} & c_{33} & 0 & 0 & 0 \\ 0 & 0 & 0 & c_{44} & 0 & 0 \\ 0 & 0 & 0 & 0 & c_{55} & 0 \\ 0 & 0 & 0 & 0 & 0 & c_{66} \end{bmatrix} \begin{bmatrix} \epsilon_1 \\ \epsilon_2 \\ \epsilon_3 \\ \epsilon_4 \\ \epsilon_5 \\ \epsilon_6 \end{bmatrix}, \quad (1)$$

where σ_i and ϵ_i represent stresses and strains, respectively, in absence of any external electric field. In wurtzite, on the other hand, one has $c_{11}=c_{22}$, $c_{13}=c_{23}$, $c_{44}=c_{55}$, and $c_{66}=(c_{11}-c_{12})/2$, leaving only five independent elastic constants Because of the close relation of the structure to wurtzite, we expect these relations to be still approximately valid. We note that all our elastic constants are calculated in the absence of electric field or polarization while experimentally, one distinguishes measurements taken at constant finite electric field or electrical displacement vector. We compare with experimental data at constant electric field.

To establish the accuracy of the computational approach, we first calculated the elastic constants and piezoelectric constants of ZnO and GaN. These results are shown in Table IV. Our calculated elastic constants for ZnO and GaN are in good agreement with previous DFT calculations (made by a more direct numerical differentiation approach of the total energies), thus establishing the accuracy of the DFPT as well as the adequate convergence of our present ABINIT calculations. They are also in good agreement with the measured values. Deviations are on the order of 15% for ZnO and 10% for GaN.

The elastic stiffness and compliance tensors of $LiGaO_2$ are given in Table V. The piezoelectric constants are also included in this table and discussed in the next section.

We can see that our calculated results show some significant deviations from Nanamatsu's experimental values. Notably, our values are systematically larger for both compressional and shear moduli. On the other hand, they are smaller than the shear moduli given by Jaffe and Berlincourt.[46] The largest discrepancies occur for c_{12} and c_{13}, which seem anomalously low in the experimental data. We note, however, that these are obtained rather indirectly from the experimental data. The directly measured quantities by Nanamatsu *et al.*[15] are given in Table VI and show a maximum deviation in compliances of 9% and in stiffnesses of 29%. A large variation in error occurs for different elastic constant combinations, which correspond to differently cut samples, indicating that the problem is at least in part experimental, since on the theory side there is no bias to obtain one coefficient more accurately than another.

We may also notice that the deviations from the hexagonal symmetry predictions are more significant for compressional moduli than for shear moduli: $c_{22}>c_{11}$ by 27% while $c_{13}\approx c_{23}$. On the other hand, $c_{55}>c_{44}$ by 19%. Comparing with ZnO and GaN, we may note that $LiGaO_2$ is significantly softer than ZnO which in turn is softer than GaN.

It is also of some interest to extract orientation averaged elastic moduli for polycrystalline materials. This gives a simpler way to compare the different materials. The Reuss average corresponds to averaging the compliances over directions while the Voigt average corresponds to averaging the stiffnesses directly. The equations for orthorhombic symmetry[47] are given below and can easily be adapted for hexagonal materials, simply by applying the additional symmetries: $c_{11}=c_{22}$, $c_{13}=c_{23}$, $c_{44}=c_{55}$, and $c_{66}=(c_{11}-c_{12})/2$ and similar equalities for the s_{ij}.

$$G_R = 15[4(s_{11}+s_{22}+s_{33}-s_{12}-s_{13}-s_{23}) + 3(s_{44}+s_{55}+s_{66})]^{-1}, \quad (2)$$

$$G_V = \frac{1}{15}(c_{11}+c_{22}+c_{33}-c_{12}-c_{13}-c_{23}) + \frac{1}{5}(c_{44}+c_{55}+c_{66}), \quad (3)$$

$$B_R = [(s_{11}+s_{22}+s_{33}) + 2(s_{12}+s_{13}+s_{23})]^{-1}, \quad (4)$$

$$B_V = \frac{1}{9}(c_{11}+c_{22}+c_{33}+2c_{12}+2c_{13}+2c_{23}). \quad (5)$$

Since the Voigt and Reuss isotropic averages of the bulk and shear moduli represent an upper and lower limit, it also makes sense to take their arithmetic average $B=(B_R+B_V)/2$ and $G=(G_R+G_V)/2$, as a better estimate of the bulk and

TABLE IV. Elastic constant (relaxed-ions) and piezoelectric coefficients in units of GPa and C/m^2, respectively, of ZnO and GaN.

		Elastic					Piezoelectric		
	Method	c_{11}	c_{12}	c_{13}	c_{33}	c_{44}	e_{31}	e_{33}	e_{15}
ZnO	Present (DFPT)	220	139	122	241	37	−0.66	1.28	−0.54
	DFPT[a]	226	139	123	242	40	−0.67	1.28	−0.53
	DFT-PW[b]						−0.51	0.89	
	DFT-LAPW[c]						−0.51	1.21	
	Hartree Fock[d]	246	127	105	246	56	−0.55	1.19	−0.46
	Expt.[e]	207	118	106	210	45	−0.62	0.96	−0.37
GaN	Present (DFPT)	345	130	95	383	91	−0.42	0.70	−0.30
	DFT-LMTO[f]	396	144	100	392	91			
	DFT-PW[g]	367	135	103	405	95			
	DFT[h]	350	140	104	376	101	−0.32	0.63	
	DFT[i]						−0.49	0.73	
	Expt.[j]	390	145	106	398	105			
	Expt.[k]						−0.55	1.12	-0.29 ± 0.02

[a]From Wu *et al.* (Ref. 30).
[b]Bernardini *et al.* (Ref. 36).
[c]Dal Corso *et al.* (Ref. 37).
[d]From Catti *et al.* (Ref. 38).
[e]Elastic constants from Kobiakov (Ref. 39) and piezoelectric constants Tokarev *et al.* (Ref. 40).
[f]From Kim *et al.* (Ref. 34).
[g]Wright *et al.* (Ref. 41).
[h]Shimada *et al.* (Ref. 42).
[i]Bernardini *et al.* (Ref. 36).
[j]Polian *et al.* (Ref. 43).
[k]Guy *et al.* (Ref. 44) and Muensit *et al.* (Ref. 45).

shear moduli of polycrystalline aggregates. One can also define an average Young's modulus $Y=(9BG)/(3B+G)$ and the Poisson's ratio $\nu=(3B-2G)/(6B-2G)$ to further characterize the average elastic behavior. The ratio of B/G is also of interest since it gives a qualitative measure of ductility: low G means low resistance to shear, hence ductility while low B means low resistance to fracture, hence brittleness. Thus high B/G indicates brittle material and a critical value from previous work appears to be a ratio of 1.75.[47] These quantities are computed using the calculated elastic and compliance tensors above and tabulated in Table VII. We also calculated the corresponding averages from the experimental data by Nanamatsu *et al.*[15] We may note that our calculated bulk modulus is significantly higher than the experimental value. Note, however that there is no direct measurement of the bulk modulus. The low values of B in the "experimental" data, result from the experimental underestimate of the shear moduli s_{12}, s_{13}, and s_{23} noted before. As a further check, we use a different method to calculate the bulk modulus of $LiGaO_2$, namely, by fitting the Vinet-Rose equation of state[48] to the energy versus volume curves. The structures were relaxed with respect to the internal degrees of freedom but c/a and b/a were kept fixed as the volume was changed. Also, as a further test, we switched from plane-wave calculations to the all electron full-potential linearized muffin-tin orbital (FP-LMTO) method[49,50] for this calculation. The result is $B=93.6$ GPa in excellent agreement with our calculations based on the elastic constants. Note that the Reuss average corresponds exactly to the usual definition of the Bulk modulus as $B=-Vdp/dV$. Our results for the bulk moduli of ZnO and GaN in Table VII also agree well with previous results extracted from equation of state fits to energy versus volume curves and to experimental data. For instance for ZnO, the experimental values range from 136 to 183 GPa.[51] For GaN, the experimental values range from 188 to 245 GPa.[34] Comparing the different materials, we can conclude that the shear moduli for $LiGaO_2$ are rather close to those of ZnO while the bulk moduli are significantly smaller. All materials studied here can be qualified as being brittle.

C. Piezoelectric constants

Several types of piezoelectric constants need to be distinguished, the first type gives the polarization in response to strain

$$P_\alpha = e_{\alpha i}\epsilon_i. \tag{6}$$

Here we use α to distinguish the Cartesian component of the polarization and i to denote the strain component in Voigt notation ($1=xx$, $2=yy$, $3=zz$, $4=yz,zy$, $5=xz,zx$, and $6=xy,yx$). The summation convention of summing over repeated indices is used. The second type of piezoelectric coefficient gives the polarization in response to stress

$$P_\alpha = d_{\alpha i}\sigma_i. \tag{7}$$

Obviously, the two are related by the elastic compliance tensor,

TABLE V. Calculated elastic constants and piezoelectric constants compared with experimental data for $LiGaO_2$.

	Present	Expt.[a]	Expt.[b]
c_{11} (GPa)	143	120	
c_{12}	75	14	
c_{13}	57	31	
c_{22}	182	140	
c_{23}	60	28	
c_{33}	154	140	160.4
c_{44}	40.5	47.4	49.8
c_{55}	48.0	57.1	56.8
c_{66}	49.7	69.0	
s_{11} (10^{-12} m^2/N)	9.58	9.1	9.0
s_{12}	−3.19	−0.5	
s_{13}	−2.30	−2.0	
s_{22}	7.37	7.3	7.1
s_{23}	−1.69	−1.4	
s_{33}	8.0	8.0	
s_{44}	24.6	21.1	
s_{55}	20.8	17.5	
s_{66}	20.1	14.5	
e_{15} (C/m^2)	−0.29	−0.34	−0.29
e_{24}	−0.30	−0.32	−0.30
e_{31}	−0.21	−0.31	
e_{32}	−0.09	−0.17	
e_{33}	0.52	0.96	0.90
d_{15} (pm/V)	−6.04	−6.0	
d_{24}	−7.41	−6.9	
d_{31}	−2.92	−4.7	
d_{32}	−0.87	−2.5	
d_{33}	4.80	8.6	

[a]From Nanamatsu *et al.* (Ref. 15).
[b]From Jaffe and Berlincourt (Ref. 46).

TABLE VI. Combinations of elastic compliances (10^{-12} m^2/N) and stiffnesses (GPa) directly measured by experiment.

	Present	Expt.[a]	Error (%)
s_{11}	9.58	9.1	5
s_{22}	7.37	7.3	1
s_{33}	8.0	8.0	0
$\frac{9s_{11}+6s_{12}+s_{22}+3s_{66}}{16}$	3.03	3.04	1
$\frac{s_{11}+6s_{13}+9s_{33}+3s_{55}}{16}$	8.13	7.6	7
$\frac{s_{22}+2s_{23}+s_{33}+s_{44}}{4}$	9.15	8.4	9
c_{44}	40.5	47.4	15
c_{55}	48.0	57.1	16
$\frac{c_{44}+c_{66}}{2}$	58.2	45.1	29

[a]Reference 15.

TABLE VII. The elastic moduli in units of GPa, the dimensionless Poisson ratio and B/G ratio.

	Calculation			Expt.[a]
Components	$LiGaO_2$	ZnO	GaN	$LiGaO_2$
G_R	46.151	41.52	105.15	55.05
G_V	46.77	46.90	108.10	56.52
B_R	94.42	160.74	190.34	60.24
B_V	95.89	147.00	190.33	66.67
G	46.46	44.21	106.63	55.78
B	95.16	153.87	190.34	60.45
Y	119.88	121.03	269.54	127.98
ν	0.58	0.74	0.53	0.294
B/G	2.05	3.48	1.79	1.08

[a]Calculated from the experimental data of Nanamatsu *et al.* (Ref. 15).

$$d_{\alpha i} = e_{\alpha j} c_{ji}^{-1} = e_{\alpha j} s_{ji}. \tag{8}$$

Alternatively, the converse piezoelectric effect shows that $d_{\alpha i}$ can also be viewed as the strain, in response to an electric field,

$$\epsilon_i = d_{i\alpha} E_\alpha. \tag{9}$$

The piezoelectric coefficients of hexagonal wurtzite ZnO and GaN are given in Table IV. In hexagonal wurtzite system with symmetry $6mm$, we have $e_{15}=e_{24}$ and $e_{31}=e_{32}$. Those of orthorhombic $LiGaO_2$ are given in Table V. For wurtzite ZnO, our results are very close to the other DFPT calculation by Wu *et al.*[30] but this is no surprise since we use the same approach and even the same code. Our results are also close to those of Bernardini *et al.*[36] for GaN and for ZnO and with those of Shimada *et al.* for GaN. Bernardini *et al.* used the Berry phase approach to calculate the polarizations but implemented the strain by a direct numerical differentiation. Here we use the Hamann *et al.*[29] linear-response or DFPT approach. Although a similar numerical strain Berry phase approach method was used by Dal Corso *et al.*[37] using a linearized augmented-plane-wave (LAPW) implementation, their values are closer to ours.

More recently, Bernardini and Fiorentini[52] calculated the d tensor directly by performing calculation of the Berry phase under finite stress. Their values for d_{31}, d_{33}, and d_{15} using LDA are −1.4, 2.7, and −3.3 pm/V. Our values can be obtained from the e tensor and the compliance matrix s and are −1.39, 2.51, and −3.29 pm/V, in excellent agreement with theirs. These authors however pointed out that the values are sensitive to the exchange-correlation potential used and differ for GGA. Their value for d_{15} in particular is −1.8 pm/V but the LDA value appears to be closer to experimental value of −3.1 pm/V.[45] This among other justifies our use of the LDA.

On the experimental side, there is also still some uncertainty on these values. For GaN, the coefficient which were actually measured are the d_{15} in Muensit *et al.*[45] and d_{33} in Guy *et al.*[44] In both cases, the strain was measured in re-

TABLE VIII. Dielectric constants of $LiGaO_2$ in different frequency ranges.

	Present	Expt.	Other
ε_1^∞	3.3424	2.99[a]	2.78[b]
ε_2^∞	3.4918	3.05	2.89
ε_3^∞	3.4904	3.05	2.89
ε_1^0	6.37		
ε_2^0	6.98		
ε_3^0	7.44		
ε_1^s	6.57	6.5[c]	6.0[d]
ε_2^s	7.23	7.5	7.0
ε_3^s	7.9	8.3	

[a]From Lenzo *et al.* (Ref. 54).
[b]From Rashkeev *et al.* (Ref. 13).
[c]From Nanamatsu *et al.* (Ref. 15).
[d]From Jaffe and Berlincourt (Ref. 46).

sponse to an external electric field, at constant stress, i.e., the converse piezoelectric effect. To obtain the values given in the table, they assumed $d_{31}=-d_{33}/2$ and the equations

$$e_{15}=d_{15}c_{44},$$

$$e_{33}=d_{33}c_{33}+2d_{31}c_{13},$$

$$e_{31}=d_{33}c_{13}+d_{31}(c_{11}+c_{12}). \tag{10}$$

The values given for e_{ij} by Guy *et al.*[44] use the elastic constants of Wright[41] to convert, so for consistency we used the same for converting their d_{15} to e_{15}. For ZnO, the values given in Table IV are the recommended values given in Ref. 53, although a range of values from different authors is given there: for instance e_{15} ranges from −0.25 to −0.59, e_{33} from 0.96 to 1.56, and e_{31} from −0.251 to −0.62.

Experimental values of e_{15} are −0.30 and −0.37 C m^{-2} for bulk GaN and ZnO, respectively, while for $LiGaO_2$ e_{15} are 0.29 and e_{24} are −0.30 C/m_2. A similar type of discrepancy appears to exist for $LiGaO_2$. While the values for e_{15} and e_{24} are in good agreement with experiment, the calculations seem to underestimate e_{33}. The d_{ij} derived from it and the compliance matrix suffers from similar discrepancies.

D. Dielectric properties

From the present calculations, we obtain several types of dielectric constants the electronic dielectric constant, ε_i^∞ and the relaxed ion dielectric constant ε_i^0, where i stands for xx, yy, and zz. Because of the orthorhombic symmetry only diagonal elements occur in the second-rank tensor. We clarify that the electronic dielectric constant corresponds to frequencies high with respect to the phonons but to energies $\hbar\omega$ well below the band gap, so not including UV interband optical transitions. They correspond in other words to the visible index of refraction squared, $n=\sqrt{\varepsilon^\infty}$. The indices of refraction in the visible were measured by Lenzo *et al.*[54] In Table VIII we compare with the values at the longest wavelengths (660 nm) given in their figure. We also compare with a calculation by Rashkeev *et al.*[13] That calculations is based on calculating $\mathrm{Im}[\varepsilon(\omega)]$ from the interband transitions and evaluating the corresponding $\mathrm{Re}[\varepsilon(0)]$ in the static limit. That calculation includes also only the electronic contributions but did not include local-field effects. As explained in the methods section, here, the ABINIT code calculates the electronic contribution from the derivative of the polarization versus electric field using the Berry phase procedure to calculate polarization and DFPT to evaluate derivatives versus static electric field. This method inherently includes local-field effects.

As for the relaxed ion dielectric constant, these pertain to the region of frequencies below the infrared. They differ from the true static dielectric constant measured say in a capacitor with dc voltage because the effects of the lattice distortion due to the piezoelectric effect are not included in it. In other words, it corresponds to the microwave frequency or far IR regime where the unit-cell deformation cannot follow the electric field, or to the clamped value at constant strain, the full static dielectric constant at constant stress (unclamped) can be written (in SI units)

$$\varepsilon_{\alpha\beta}^s=1+\chi_{\alpha\beta}^{elec}+\chi_{\alpha\beta}^{phon}+\chi_{\alpha\beta}^{piezo} \tag{11}$$

with

$$\chi_{\alpha\beta}^{piezo}=\frac{1}{\epsilon_0}\frac{\partial P_\alpha}{\partial \eta_i}\frac{\partial \eta_i}{\partial E_\beta}=\frac{1}{\epsilon_0}e_{\alpha i}d_{\alpha i} \tag{12}$$

with ϵ_0 the permittivity of the vacuum.

The relaxed ion dielectric constant, labeled ε^0 omits only the last term in Eq. (11). The values of the dielectric tensor components corresponding to different frequencies are given in Table VIII.

We note that our calculated ϵ^∞ are larger than the measured ones at 660 nm. This may in part be because the LDA underestimates the gap and hence overestimates the electronic screening. In part, it may also be related to the downward bending of the dielectric constants as we start approaching the phonon region. Comparison to Rashkeev *et al.*'s results[13] gives some indication of the importance of local-field effects although it may in part also result from the use of a different band-structure approach. In agreement with experiment, both calculations predict the xx component to be smaller than the yy and zz components, which in turn are quite close to each other. Interestingly, while the structure is derived from wurtzite in which one would have expected the xx and yy components to be closer and different from the zz component, it is the xx component that stands out making the material approximately biaxial.

The static dielectric constants are found to be within 5% of the experimental values reported by Nanamatsu *et al.*[15] The piezoelectric contribution is rather small, only of order 0.2–0.4.

E. Vibrational modes and infrared spectra

1. Symmetry considerations

As $LiGaO_2$ belongs to the point group C_{2v}, it has optically active modes corresponding to the irreducible representations a_1, b_1, and b_2. The latter have the same symmetry as a

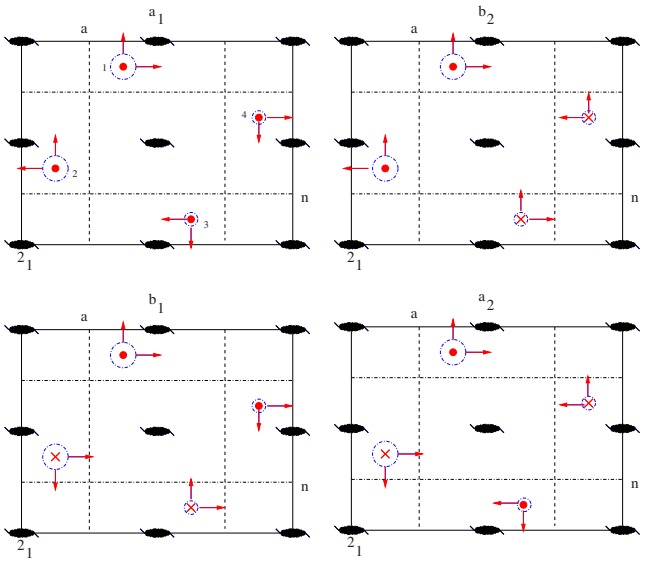

FIG. 2. (Color online) Displacement patterns for modes of different symmetry. The symmetry elements are indicated. The spheres indicate the positions of one type of atom (say the Li atom) with large spheres in the bottom plane and the small sphere in the plane $c/2$ higher.

vector along z, x, and y, respectively, chosen along the c, a, and b axes of the crystal and thus couple to electric fields in these directions. The other irreducible representation a_2 is Raman but not infrared active.

To guide further discussions, we show the symmetry character of the mode displacement in Fig. 2. For each type of atom, there are four equivalent atoms in the unit cell, as indicated. Their x, y, and z displacements are related to each other as indicated for each irreducible symmetry. For example, in an a_1 mode the z motions of all four atoms are in the same direction but the atoms 1 and 2 (see figure) have opposite x motions because these two atoms are related by a glide mirror plane (indicated in the figure by the vertical dashed line and labeled "a") with translation by $b/2$, perpendicular to x (which is horizontal) and the a_1 mode pattern must be even under this mirror plane. However, this mirror operation turns x in to $-x$. Atoms 1 and 4 move in the same direction because they are related by a glide mirror plane of the type n (indicated by the dashed-dotted lines) with both an $(\mathbf{a}+\mathbf{c})/2$ translation. This operation is perpendicular to y so it leaves x invariant in a symmetric pattern. Atom 3 has opposite x motion to atom 1 because the two are related by a twofold screw axis (2_1) which turns x into $-x$. These labels of the symmetry elements explain the space-group notation $Pna2_1$. Now, within these symmetry constraints the motions of the four types of atoms (Li, Ga, O_I, and O_{II}) of atoms can still be rather complex as we will discuss below.

Since there are 16 atoms in the cell, there are in total 48 modes. Removing the zero-frequency "acoustic modes" corresponding to a pure translation along z, x, or y at the Brillouin-zone center, we retain the optical modes

$$\Gamma = 11a_1 + 12a_2 + 11b_1 + 11b_2. \tag{13}$$

2. Mode frequencies and infrared spectra

The calculated phonon frequencies at Γ for $LiGaO_2$ are shown in Table IX. They are compared with the experimental data from Knoll and Kuzmany[14] or more precisely the supplementary data provided with that reference. They were extracted from a combination of Raman and infrared reflectivity spectra. While for some modes the agreement is rather good, others show significant deviations. We emphasize that the individual mode frequencies are ultimately extracted from the data by means of an oscillator model and involve a rather complex fitting procedure to the data. We therefore need to make the comparison more directly in terms of the spectra predicted by our calculations.

One of the most widely used methods to measure phonons is infrared absorption. The oscillator strengths are calculated from[28]

$$S_{n,\alpha\alpha} = \left| \sum_{\kappa} Z^*_{\kappa,\alpha\alpha} U_n(\kappa,\alpha) \right|^2 \tag{14}$$

with $Z^*_{\kappa,\alpha\beta} = V\partial P_\alpha / \partial \tau_{\kappa\beta}(\mathbf{q}=0)$ the Born effective charge tensor components, $U_n(\kappa,\alpha)$ the eigenvector for mode n in

TABLE IX. Calculated zone-center phonon frequencies (in cm^{-1}) and oscillator strengths (in atomic units) in $LiGaO_2$. The numbers in parentheses are experimental data from Knoll and Kuzmany (Ref. 14).

a_2	b_{1T}	b_{1L}	S^{b1}_{xx}	b_{2T}	b_{2L}	S^{b2}_{yy}	a_{1T}	a_{1L}	S^{a1}_{zz}
129.8 (244.0)	199.2 (205.0)	201.2 (207.0)	1.0×10^{-5}	130.1 (140.3)	130.1 (140.3)	5.2×10^{-8}	119.5 (129.5)	119.6 (129.5)	4.7×10^{-8}
144.2 (290.0)	235.5 (251.0)	236.7 (252.0)	6.7×10^{-6}	197.4 (204.7)	197.6 (204.7)	9.1×10^{-7}	201.7 (219.5)	201.9 (219.5)	1.4×10^{-6}
241.6 (324.0)	319.6 (320.0)	323.9 (322.0)	3.9×10^{-5}	294.0 (301.0)	305.3 (302.5)	1.2×10^{-4}	247.4 (253.0)	247.5 (253.0)	3.0×10^{-7}
281.5 (408.0)	360.0 (364.0)	361.3 (366.0)	1.3×10^{-5}	312.5 (314.5)	316.1 (322.0)	1.3×10^{-5}	295.7 (309.5)	312.1 (324.5)	1.6×10^{-4}
313.7 (437.0)	442.2 (407.0)	442.2 (411.0)	2.8×10^{-7}	447.1 ((324.0)	468.2 (324.0)	3.9×10^{-4}	434.4 (388.2)	439.5 (407.3)	1.5×10^{-4}
441.6 (480.0)	470.8 (434.0)	475.1 (446.0)	1.1×10^{-4}	476.4 (406.5)	477.3 (435.0)	9.2×10^{-6}	453.0 (408.0)	460.7 (425.0)	1.6×10^{-4}
452.1 (487.0)	481.8 (504.0)	482.6 (515.0)	1.5×10^{-5}	485.6 (451.5)	492.5 (472.0)	7.3×10^{-5}	473.8 (445.0)	479.3 (445.0)	1.0×10^{-4}
476.8 (504.0)	529.3 (515.5)	548.1 (535.0)	9.8×10^{-4}	517.8 (494.0)	552.9 (502.0)	2.8×10^{-4}	505.7 (493.2)	509.8 (502.5)	3.1×10^{-4}
509.0 (558.0)	548.1 (536.0)	605.4 (586.0)	9.6×10^{-7}	564.9 (503.0)	566.6 (537.0)	6.4×10^{-6}	514.2 (503.2)	579.6 (573.0)	3.3×10^{-4}
560.2 (647.0)	639.8 (657.5)	694.9 (708.0)	2.7×10^{-4}	638.7 (656.5)	678.6 (704.0)	5.6×10^{-4}	627.6 (644.8)	628.8 (646.0)	8.0×10^{-5}
633.8 (655.0)	696.2 (723.0)	741.3 (768.0)	5.5×10^{-6}	686.2 (714.0)	762.3 (776.0)	8.3×10^{-5}	633.3 (655.0)	737.1 (757.5)	3.0×10^{-4}
699.6 (721.0)									

TABLE X. Born effective charge tensor components in $LiGaO_2$.

	Li	Ga	O_I	O_{II}
x	1.0207	2.5394	−1.7786	−1.7815
y	0.9529	2.7772	−2.2325	−1.4976
z	1.0034	2.7731	−1.5218	−2.2448

which κ labels the atom, and α the Cartesian directions. P_α is the polarization, V the volume of the unit cell, and $\boldsymbol{\tau}_\kappa$ the position of the κth atom. Note that because of the orthorhombic symmetry $Z^*_{\kappa.\alpha\beta}$ has only diagonal elements. For $\alpha=z$, x, and y the oscillator strengths are only nonzero for a_1, b_1, and b_2 modes, respectively. The calculated Born effective charges are given in Table X.

In terms of these oscillator strengths, the dielectric function is given by

$$\varepsilon_{\alpha\alpha}(\omega) = \varepsilon^{\infty}_{\alpha\alpha} + \frac{4\pi}{V}\sum_n \frac{S_{n,\alpha\alpha}}{\omega_n^2 - \omega^2 - i\Gamma_n\omega}, \tag{15}$$

where ω_n and Γ_n are the mode frequencies and damping factors, respectively. For the latter we assume a constant value of 5 cm^{-1} except for the b_2 modes for which we use the mode-dependent experimental values given in Ref. 14. They are similar in magnitude.

The transverse modes are given by the peaks in $\mathrm{Im}[\varepsilon(\omega)]$ and the longitudinal modes are given by the peaks in $\mathrm{Im}[-\varepsilon^{-1}(\omega)]$ which are shown in Fig. 3. Experimentally, the directly measured quantity by Knoll and Kuzmany[14] is the normal-incidence infrared reflectivity, given by

$$R = |(n-1)/(n+1)|^2, \tag{16}$$

where the index of refraction n is the square root of the complex dielectric function $n=\sqrt{\epsilon(\omega)}$. We thus compare our calculated reflectivity with the experimental data by Knoll and Kuzmany.[14] The experimental curves in the lower panel of Figs. 4–6 are reproduced from the their figure.

We now discuss the nature of the modes. In wurtzite, there are three "quasiacoustic" modes, E_2^{low} (Raman active) and B_1^{low} (silent). These can be thought of as zone-boundary (L) phonons in zinc blende folded to the Γ point. Their characteristic is that the two molecules in the unit cell move in antiphase to each other. In the $LiGaO_2$ structure, with four times as many atoms, one expects 12 modes of this type. While E_2 becomes a_1+a_2 and B_1 becomes b_1, there are also modes that in wurtzite lie at the zone boundary which now appear as zone-center modes. Thus, we cannot exactly predict from symmetry considerations how many modes or each symmetry are weak quasiacoustic modes. For example, it appears that the third b_2 mode and fourth a_1 mode are already true optic modes with strong oscillator strength.

For a_1 symmetry the reflectivity consists of several clearly distinguishable bands. The lowest one is at 300 cm^{-1} and has pretty high intensity for such a low mode. Then appear three evenly spread modes between 400 and 500 cm^{-1} followed by a strong pair of modes slightly above 500 cm^{-1} and another pair of modes at about 630 cm^{-1} of which one has a strong oscillator strength. This leads to several clearly defined reststrahlen bands in the reflectivity. One can clearly see how the up-swing of each reflectivity band corresponds to the corresponding transverse mode and the down-swing to the longitudinal mode. In the experiment, the three peaks which we find between 350 and 500 cm^{-1} seem to occur at

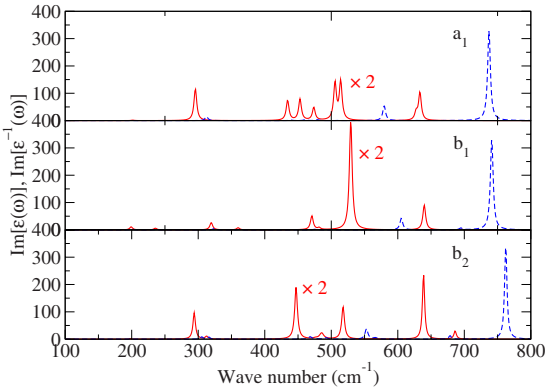

FIG. 3. (Color online) Calculated infrared spectra, $\mathrm{Im}[\varepsilon(\omega)]$ (red solid line) and $\mathrm{Im}[-1/\varepsilon(\omega)]$ (blue dashed): (a) a_1, (b) b_1, and (c) b_2.

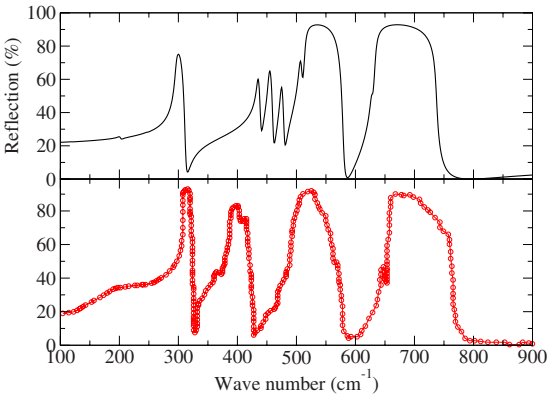

FIG. 4. (Color online) Comparison of experimental (lower panel) infrared reflectivity of $a_1(Z)$ with calculated (upper panel) reflectivity.

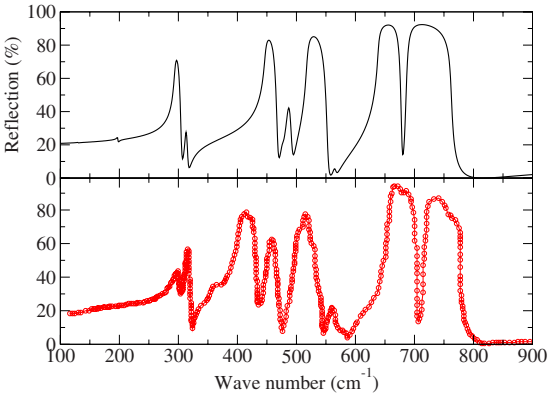

FIG. 5. (Color online) Comparison of experimental (lower panel) infrared reflectivity of $b_1(y)$ with calculated (upper panel) reflectivity.

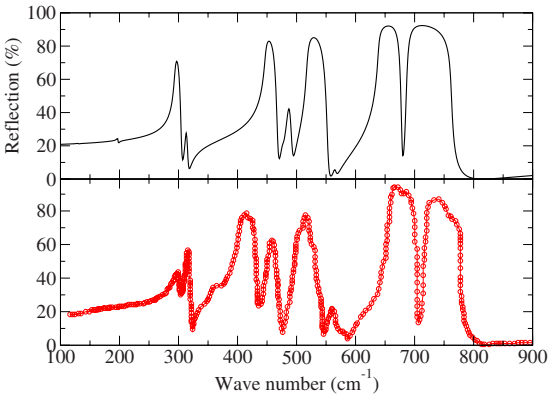

FIG. 6. (Color online) Comparison of experimental (lower panel) infrared reflectivity of $b_2(x)$ with calculated (upper panel) reflectivity.

significantly lower frequency, namely, between 350 and 425 cm^{-1} and appear to be closer together, although one can still recognize three features in it. The higher two bands and the low-frequency 300 cm^{-1} band are in much better agreement between theory and experiment.

For b_1 symmetry, the visual agreement between the spectra is excellent. Again, the spectrum can roughly be divided in three regions, a low-frequency mode near 300 cm^{-1} followed by a three peak region between 400 and 550 cm^{-1} and a high-frequency band between 600 and 800 with a sharp dip in the middle. The spectrum for b_2 symmetry is qualitatively very similar to that for b_1 symmetry. In both cases, we note that the features in the middle range (350–550 cm^{-1}) are somewhat shifted up relative to the experiment while for the high-frequency range, the theory seems to underestimate slightly the experimental frequencies. Note, for example, the position of the sharp dip in reflectivity.

3. Further discussion of vibrational modes

To gain further insight, we inspect the mode eigenvectors. All the modes have a rather mixed character, making it difficult to assign a clear signature to them. An example, Fig. 7

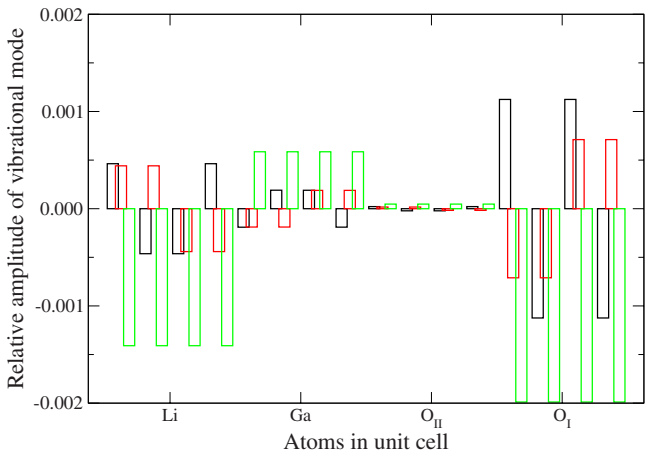

FIG. 7. (Color online) Displacements in x (black or left), y (red or middle), and z (green or right) for each atom in the unit cell for mode a_{1T}^4 as discussed in the text.

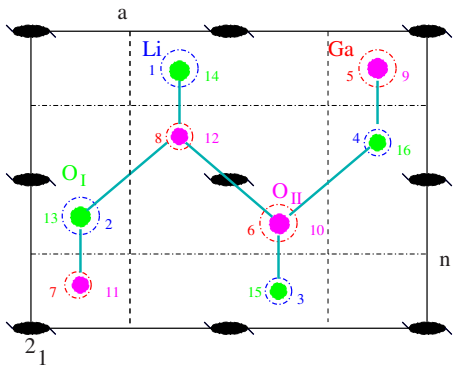

FIG. 8. (Color online) Atom numbering in the unit cell corresponding to Figs. 7–12. Large open circles represent Li (1-4) and Ga (5-8) as indicated and small filled spheres represent O_I (9-12) and O_{II} (13-16) atoms sitting on top of cations. Larger spheres of Li (1,2) and Ga (5,6) lie in bottom plane, smaller spheres Li (3,4) and Ga (7,8) lie in upper basal plane.

shows the displacements on the different atoms in the cell in x, y, and z directions for the fourth a_{1T} mode at 295.7 cm^{-1}. The x displacements are shown as black bars, the y displacements as red bars, and the z displacements as green bars (ordered from left to right) for each atom. The first four atoms are Li, the next four are Ga, and so on as indicated on the x axis. The positions of atom numbers (1–16) in the cell are shown in Fig. 8. One can see that the Li and O_I (which is above each corresponding Li) all move in phase in the z direction. Also, the Ga and O_{II} move in phase but opposite to the Li and O_I. The fact that all four atoms of the same type move in phase is consistent with a_1 symmetry as mentioned earlier in connection with Fig. 2. The fact that Li and O_I move in phase means that this is a low-frequency mode in which molecules Li-O_I move against Ga-O_{II} rather than atoms moving against each other in each bond. The strongest z motions are on Li and O_I. Nonetheless, the displacement of O_I is larger than that of Li and thus there is a bit of bond compression and stretching and this explains why it can have a significant oscillator strength. In the Ga-O_{II} bonds in the z direction, in this low-frequency mode essentially only Ga moves because it is much heavier than O. The displacements in x and y directions can be checked to be consistent with a_1 symmetry. For instance Li^1 moves opposite to Li^2. Further considering the x motions, one can see for instance that atoms Li^1 and O_I^3, which are nearest neighbors to each other also move in the same direction. So, overall, in this mode the molecules move against each other, however, because of the unequal displacements of Li and O_I and Ga and O_{II} some bond stretching occurs and gives the mode a rather strong oscillator strength.

Figure 9 shows the highest a_{1L}^{11} mode, displayed in similar fashion. In this case, we see that the motion is predominantly in the z direction but now Li and O_I and Ga and O_{II} move opposite to each other. O_I sits right on top of Li and O_{II} on top of Ga while Li and Ga move in phase with each other and O_I moves in phase with O_{II}. So, this is mostly a bond stretch mode in the c direction as expected. The largest amplitudes occur on the Li and the O_{II}. As expected for this high-frequency mode, in the bond stretch, the lightest atom

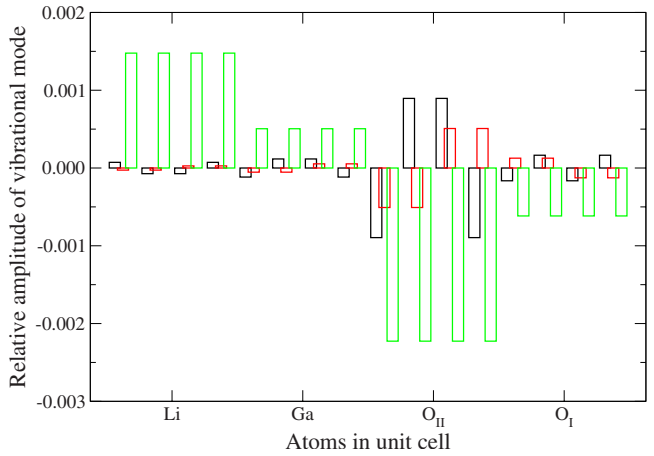

FIG. 9. (Color online) Displacements in x (black or left), y (red or middle), and z (green or right) for each atom in the unit cell for mode a_{1L}^{11} as discussed in the text.

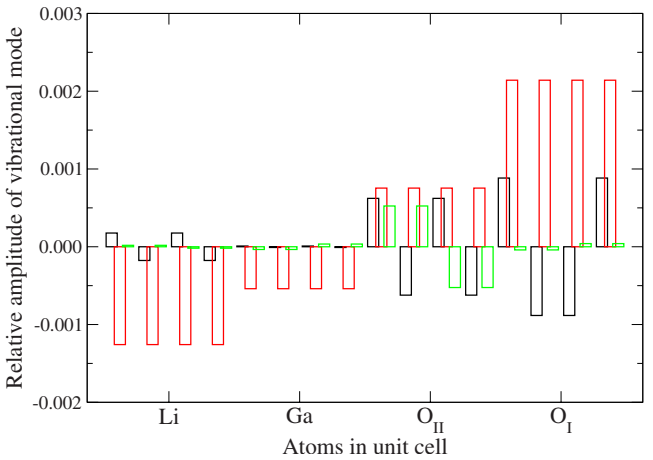

FIG. 11. (Color online) Displacements in x (black or left), y (red or middle), and z (green or right) for each atom in the unit cell for mode b_{2L}^{11} as discussed in the text.

has the largest displacement. One can however also see significant x and y displacements on O_{II} in this mode and one can check that they correspond also to stretches of the bonds with the nearest neighbors. Thus, although this mode could be said to be derived mostly from an A_{1L} wurtzite type mode, it is does not purely have this character.

The highest transverse optical mode of a_1 symmetry has a rather different eigenvector as can be seen in Fig. 10. One can still see the Ga-O_{II} stretch in the z direction. The eigenvectors for corresponding longitudinal and transverse modes are not purely dictated by symmetry in this material and thus there is no need for the corresponding modes to have the same eigenvectors.

The eigenvector of b_{2L}^{11} is shown in Fig. 11. As expected, this mode is strongly polarized in the y direction and therefore has a strong coupling to an electric field in that direction. One sees again all atoms of the same type move in phase in the y direction. Li^1 is bonded to atoms O_I^3 and O_{II}^3 and O_{II}^4 in its basal plane and O_I^2 above it. One can see that the displacements of the basal plane oxygen atoms in the y direction are all opposite to that of Li^1. So, this mode has a strong E_{1L} wurtzite type character. Consistent with the ordering of modes in ZnO, $\omega(E_{1L}) > \omega(A_{1L})$, we also find in $LiGaO_2$ that the mostly in-plane b_{1L} and b_{2L} modes are slightly higher than the a_{1L} mode. But again, the mode is not pure, some x- and z-like motions are mixed in, mostly on O_{II}.

We now examine a mode a_{1T}^8 at 505 cm^{-1} as shown in Fig. 12. Focusing on the x motions and isolating part of the structure, we see that locally around atom Li^1 it looks as shown schematically in Fig. 13. So, this corresponds to a stretching of in-plane bonds but the upper layer is in antiphase with the lower layer. This is characteristic of an E_2^{high} wurtzite type mode. This is consistent with its frequency being between that of the typical transverse optical modes and the longitudinal optical modes. On the other hand, there are significant z motions in this mode similar to the high frequency a_{1L}^{11} with Ga-O_{II} and Li-O_O stretch character. So one could say it is some mixture of wurtzite A_1 and E_2 and this gives it a net dipolar character whereby it has a strong oscillator strength for coupling to electric fields in the z direction.

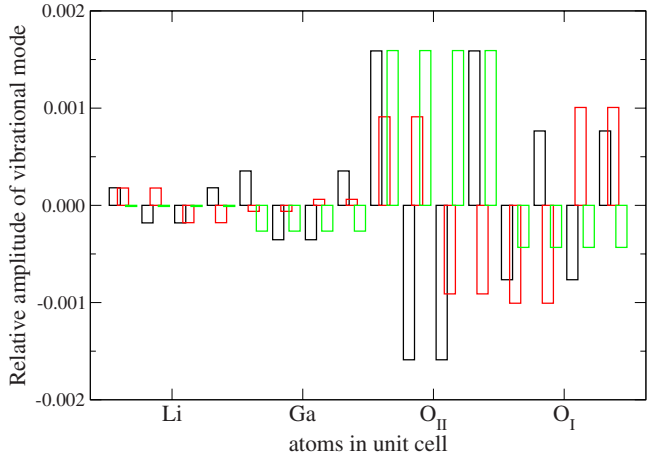

FIG. 10. (Color online) Displacements in x (black or left), y (red or middle), and z (green or right) for each atom in the unit cell for mode a_{1T}^{11} as discussed in the text.

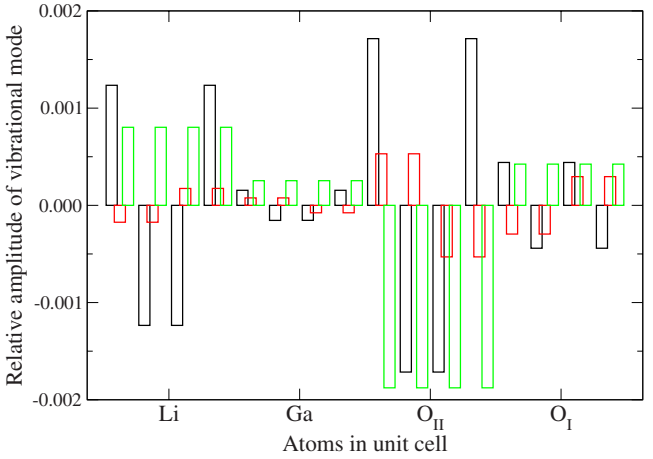

FIG. 12. (Color online) Displacements in x (black or left), y (red or middle), and z (green or right) for each atom in the unit cell for mode a_{1T}^8 as discussed in the text.

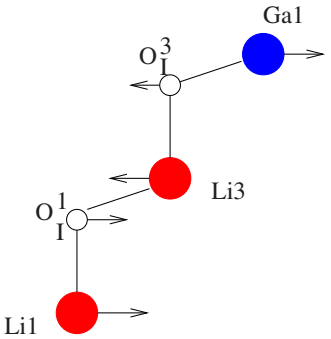

FIG. 13. (Color online) Schematic sketch of x motions in mode a_{1T}^{8}.

One could further analyze the many remaining modes in a similar fashion but in summary we can just conclude that the low symmetry leads to a significant interaction of the basic modes of wurtzite so that they are barely recognizable. It is only after in-depth inspection that one can recognize some correspondence to wurtzite like modes. For example, the E_2^{high} wurtzite like mode (which in wurtzite is only Raman active) splits into a_1 and a_2 modes and thus the a_1 component now has significant interaction with other a_1 modes and becomes infrared active. As expected, high-frequency modes correspond to bond stretch modes of the cation-anion bonds but one cannot clearly distinguish pure Li-O and pure Ga-O bond stretch modes. Low-frequency modes have a quasiacoustic zone-boundary character in which molecules vibrate against each other.

IV. CONCLUSIONS

In summary, a comprehensive computational study was carried out of the structural and lattice-dynamical properties of $LiGaO_2$. Throughout this paper, we compared the calculated results for $LiGaO_2$ with those of ZnO and GaN (which were also recalculated here). The lattice constants of $LiGaO_2$ agree with experiment to better than 2%. The elastic constants for ZnO and GaN agree generally with experimental values and prior calculations to within 15% and 10%, respectively. Part of these discrepancies are probably due to the underestimation of the lattice constants (overbinding) of LDA while part of the discrepancy may also result from variations in experimental samples. For $LiGaO_2$ our calculated compliances agree within 10% with all directly measured experimental values while for the elastic stiffnesses, the discrepancies are between 15% and 30% with the one experimental study that determined the full set of elastic constants. Some individual elastic constants, notably c_{12} and c_{13} show a large deviation from the values reported in the literature but we notice that these are derived from the data in an indirect manner and are therefore subject to a larger uncertainty.

There remains also significant uncertainty on piezoelectric constants in all of these materials with our calculated values falling well within the range of previous computational and experimental values. Both the high-frequency dielectric constants, relevant to the optical properties in the visible and near IR and the static dielectric constants agree well with experiment. We included the small piezoelectric contribution to the static dielectric constants. Curiously, in terms of anisotropy and in agreement with experiment, one finds one of the in-plane directions to stand out more from the other two directions than the c direction in spite of the close connection of this crystal structure to the hexagonal wurtzite structure.

The infrared reflectivity spectra are well reproduced by our calculations although again, there are disagreements on individual modes probably resulting from the complex fitting procedure involved in assigning the modes via an oscillator model. The nature of the modes was discussed. We find that the mode patterns are complex with Li-O and Ga-O bond stretches significantly mixed as well as a significant mixing of z motion and in-plane motions. This is different from wurtzite where the high symmetry leads to A_1 and B_1 symmetries being purely z-like and E_1, E_2 modes being purely in plane. The only thing one can say is that the highest frequency modes show a clear strong dipolar character in each bond whereas the lower frequency modes are characterized by in-phase motion of nearest-neighbor atoms.

ACKNOWLEDGMENTS

A. Boonchun wishes to thank the Commission of Higher Education of Thailand for support. The calculations were performed at the CWRU HPC cluster. Support from the National Science Foundation under Grant No. DMR-0710485 is acknowledged.

[1] K. Sakurada, A. Kobayashi, Y. Kawaguchi, J. Ohta, and H. Fujioka, Appl. Phys. Lett. **90**, 211913 (2007).
[2] S. W. Seo, K. K. Lee, S. Kang, S. Huang, W. A. Doolittle, N. M. Jokerst, and A. S. Brown, Appl. Phys. Lett. **79**, 1372 (2001).
[3] S. Kang, W. A. Doolittle, A. S. Brown, and S. R. Stock, Appl. Phys. Lett. **74**, 3380 (1999).
[4] J. D. MacKenzie, S. M. Donovan, C. R. Abernathy, S. J. Pearton, P. H. Holloway, R. Linares, J. Zavada, and B. Chai, J. Electrochem. Soc. **145**, 2581 (1998).
[5] C.-H. Chen, J.-Y. Yu, T.-H. Huang, L. Chang, and M. Chou, ECS Trans. **28**, 33 (2010).
[6] T. Ishii, Y. Tazoh, and S. Miyazawa, J. Cryst. Growth **186**, 409 (1998).
[7] I. Ohkubo, C. Hirose, K. Tamura, J. Nishii, H. Saito, H. Koinuma, P. Ahemt, T. Chikyow, T. Ishii, S. Miyazawa, Y. Segawa, T. Fukumura, and M. Kawasaki, J. Appl. Phys. **92**, 5587 (2002).
[8] J. T. Wolan and G. B. Hoflund, J. Vac. Sci. Technol. A **16**, 3414 (1998).
[9] C. H. Hsu, K. P. Ip, J. W. Johnson, S. N. G. Chu, O. Kryliouk, S. J. Pearton, L. Li, B. H. T. Chai, T. J. Anderson, and F. Ren, Electrochem. Solid-State Lett. **4**, C35 (2001).
[10] T. S. Cheng, C. T. Foxon, and S. V. Novikov, Semiconductors

30, 603 (1996).
[11] T. Omata, K. Tanaka, A. Tazuke, K. Nose, and S. Otsuka-Yao-Matsuo, J. Appl. Phys. **103**, 083706 (2008).
[12] R. C. Miller, W. A. Nordland, E. D. Kolb, and W. L. Bond, J. Appl. Phys. **41**, 3008 (1970).
[13] S. N. Rashkeev, S. Limpijumnong, and W. R. L. Lambrecht, J. Opt. Soc. Am. B **16**, 2217 (1999).
[14] P. Knoll and H. Kuzmany, Phys. Rev. B **29**, 2221 (1984).
[15] S. Nanamatsu, K. Doi, and M. Takahashi, Jpn. J. Appl. Phys. **11**, 816 (1972).
[16] S. N. Gupta, J. F. Vetelino, V. B. Jipson, and J. C. Field, J. Appl. Phys. **47**, 858 (1976).
[17] S. Limpijumnong, W. R. L. Lambrecht, B. Segall, and K. Kim, in *III-V Nitrides*, MRS Symposia Proceedings Vol. 449, edited by F. A. Ponce, T. D. Moustakas, I. Aakasak, and B. A. Monemar (Materials Research Society, Pittsburgh, 1997), pp. 905–910.
[18] T. J. Peshek, T. R. Paudel, K. Kash, and W. R. L. Lambrecht, Phys. Rev. B **77**, 235213 (2008).
[19] T. R. Paudel and W. R. L. Lambrecht, Phys. Rev. B **78**, 115204 (2008).
[20] T. R. Paudel and W. R. L. Lambrecht, Phys. Rev. B **79**, 245205 (2009).
[21] T. R. Paudel and W. R. L. Lambrecht, Phys. Rev. B **76**, 115205 (2007).
[22] P. Hohenberg and W. Kohn, Phys. Rev. **136**, B864 (1964).
[23] W. Kohn and L. J. Sham, Phys. Rev. **140**, A1133 (1965).
[24] M. C. Payne, M. P. Teter, D. C. Allan, T. A. Arias, and J. D. Joannopoulos, Rev. Mod. Phys. **64**, 1045 (1992).
[25] X. Gonze, J.-M. Beuken, R. Caracas, F. Detraux, M. Fuchs, G.-M. Rignanese, L. Sindic, M. Verstraete, G. Zerah, F. Jollet, M. Torrent, A. Roy, M. Mikami, Ph. Ghosez, J.-Y. Raty, and D. C. Allan, Comput. Mater. Sci. **25**, 478 (2002).
[26] S. Baroni, P. Giannozzi, and A. Testa, Phys. Rev. Lett. **58**, 1861 (1987).
[27] X. Gonze, Phys. Rev. B **55**, 10337 (1997).
[28] X. Gonze and C. Lee, Phys. Rev. B **55**, 10355 (1997).
[29] D. R. Hamann, X. Wu, K. M. Rabe, and D. Vanderbilt, Phys. Rev. B **71**, 035117 (2005).
[30] X. Wu, D. Vanderbilt, and D. R. Hamann, Phys. Rev. B **72**, 035105 (2005).
[31] J. P. Perdew and A. Zunger, Phys. Rev. B **23**, 5048 (1981).
[32] M. Fuchs and M. Scheffler, Comput. Phys. Commun. **119**, 67 (1999).
[33] M. Marezio, Acta Crystallogr. **18**, 481 (1965).
[34] K. Kim, W. R. L. Lambrecht, and B. Segall, Phys. Rev. B **53**, 16310 (1996).
[35] T. R. Paudel and W. R. L. Lambrecht, Phys. Rev. B **77**, 205202 (2008).
[36] F. Bernardini, V. Fiorentini, and D. Vanderbilt, Phys. Rev. B **56**, R10024 (1997).
[37] A. Dal Corso, M. Posternak, R. Resta, and A. Baldereschi, Phys. Rev. B **50**, 10715 (1994).
[38] M. Catti, Y. Noel, and R. Dovesi, J. Phys. Chem. Solids **64**, 2183 (2003).
[39] J. B. Kobiakov, Solid State Commun. **35**, 305 (1980).
[40] E. E. Tokarev, I. B. Kobyakov, I. P. Kaz'mina, A. N. Lobachev, and G. S. Pado, Fiz. Tverd. Tela (Leningrad) **17**, 980 (1975) [Sov. Phys. Solid State **17**, 629 (1975)].
[41] A. F. Wright, J. Appl. Phys. **82**, 2833 (1997).
[42] K. Shimada, T. Sota, and K. Suzuki, J. Appl. Phys. **84**, 4951 (1998).
[43] A. Polian, M. Grimsditch, and I. Grzegory, J. Appl. Phys. **79**, 3343 (1996).
[44] I. L. Guy, S. Muensit, and E. M. Goldys, Appl. Phys. Lett. **75**, 4133 (1999).
[45] S. Muensit, E. M. Goldys, and I. L. Guy, Appl. Phys. Lett. **75**, 3965 (1999).
[46] H. Jaffe and D. A. Berlincourt, Proc. IEEE **53**, 1372 (1965).
[47] P. Ravindran, L. Fast, P. A. Korzhavyi, B. Johansson, J. Wills, and O. Eriksson, J. Appl. Phys. **84**, 4891 (1998).
[48] P. Vinet, J. Ferrante, J. R. Smith, and J. H. Rose, J. Phys. C **19**, L467 (1986).
[49] M. Methfessel, M. van Schilfgaarde, and R. A. Casali, in *Electronic Structure and Physical Properties of Solids. The Use of the LMTO Method*, Lecture Notes in Physics Vol. 535, edited by H. Dreyssé (Springer-Verlag, Berlin, 2000), p. 114.
[50] T. Kotani and M. van Schilfgaarde, Phys. Rev. B **81**, 125117 (2010).
[51] F. Decremps, F. Datchi, A. M. Saitta, A. Polian, S. Pascarelli, A. Di Cicco, J. P. Itié, and F. Baudelet, Phys. Rev. B **68**, 104101 (2003).
[52] F. Bernardini and V. Fiorentini, Appl. Phys. Lett. **80**, 4145 (2002).
[53] *Elastic, Piezo-electric, Pyro-electric, Piezo-optic, Electro-optic Constants and Nonlinear Dielectric Susceptibilities of Crystals*, Landolt-Börnstein, New Series, Group III Vol. 11, edited by K. H. Hellwege (Springer, Berlin, 1979).
[54] P. V. Lenzo, E. G. Spencer, and J. P. Remeika, Appl. Opt. **4**, 1036 (1965).